LETTER • OPEN ACCESS

Observational constraints on the effective climate sensitivity from the historical period

View the article online for updates and enhancements.

Environmental Research Letters

LETTER

Observational constraints on the effective climate sensitivity from the historical period

Katarzyna B Tokarska[1,5] , Gabriele C Hegerl[1] , Andrew P Schurer[1] , Piers M Forster[2] and Kate Marvel[3,4]

[1] School of Geosciences, University of Edinburgh, United Kingdom
[2] University of Leeds, United Kingdom
[3] NASA Goddard Institute for Space Studies, New York, NY, United States of America
[4] Department of Applied Physics and Applied Mathematics, Columbia University, New York, NY, United States of America
[5] Current affiliation: Institute for Atmospheric and Climate Science, ETH Zurich, Zurich, Switzerland

E-mail: kasia.tokarska@ed.ac.uk

Abstract

The observed warming in the atmosphere and ocean can be used to estimate the climate sensitivity linked to present-day feedbacks, which is referred to as the effective climate sensitivity (S_{hist}). However, such an estimate is affected by uncertainty in the radiative forcing, particularly aerosols, over the historical period. Here, we make use of detection and attribution techniques to derive the surface air temperature and ocean warming that can be attributed directly to greenhouse gas increases. These serve as inputs to a simple energy budget to infer the likelihood of S_{hist} in response to observed greenhouse gases increases over two time periods (1862–2012 and 1955–2012). The benefit of using greenhouse gas attributable quantities is that they are not subject to uncertainties in the aerosol forcing (other than uncertainty in the attribution to greenhouse gas versus aerosol forcing not captured by the multi-model aerosol response pattern). The resulting effective climate sensitivity estimate, S_{hist}, ranges from 1.3 °C to 3.1 °C (5%–95% range) over the full instrumental period (1862–2012) for our best estimate, and gets slightly wider when considering further uncertainties. This estimate increases to 1.7 °C–4.6 °C if using the shorter period (1955–2012). We also evaluate the climate model simulated surface air temperature and ocean heat content increase in response to greenhouse gas forcing over the same periods, and compare them with the observationally-constrained values. We find that that the ocean warming simulated in greenhouse gas only simulations in models considered here is consistent with that attributed to greenhouse gas increases from observations, while one model simulates more greenhouse gas-induced surface air warming than observed. However, other models with sensitivity outside our range show greenhouse gas warming that is consistent with that attributed in observations, emphasising that feedbacks during the historical period may differ from the feedbacks at CO_2 doubling and from those at true equilibrium.

1. Motivation

The ultimate warming of the climate system in response to a doubling of atmospheric CO_2 concentration from preindustrial, and once the system reaches an equilibrium, is known as the equilibrium climate sensitivity (ECS), and is likely to range from 1.5 °C to 4.5 °C (17%–83% probability), as assessed by the Fifth Assessment Report of the Intergovernmental Panel on Climate Change (IPCC AR5 2013). However, the historical and present-day state of the climate system that we can observe is not at equilibrium yet. The global ocean stores more than 90% of the Earth's energy imbalance, taking centuries to reach equilibrium (Hansen *et al* 2011, Church *et al* 2013). We refer to the climate sensitivity inferred from the historical and present-day conditions as the *effective* climate sensitivity (S_{hist}), which may be different from climate

sensitivity at equilibrium (Knutti *et al* 2017, Rugenstein *et al* 2019), due to slow response additional climate feedbacks that come into play on longer timescales and when the pattern of global warming is fully developed (including, for example, sea ice retreat). (Note that the Earth system sensitivity that includes the response to ice sheet melt and release of CO_2 from permafrost may be even higher; Knutti *et al* 2017.) Furthermore, the strength of some feedbacks, such as the cloud feedback, may change over time and at higher levels of warming (Knutti *et al* 2017, Dessler and Forster 2018). Nevertheless, observations during the historical period (here defined as 1862–2012) provide us with useful information, allowing us to constrain important aspects of the climate model responses (Forster 2016, Knutti *et al* 2017).

There are multitudes of estimates of climate sensitivity summarised in Knutti *et al* (2017), many of which are based on estimates of feedbacks and analysis of climate models (summarised in Knutti *et al* 2017—figure 1 therein with red bars: e.g. Harris *et al* 2013, van Hateren 2013, Shindell 2014, Millar *et al* 2015). Other estimates of climate sensitivity arise from observations over the historical period (e.g. Gregory *et al* 2002, Frame *et al* 2005, Otto *et al* 2013, Johansson *et al* 2015, Forster 2016, Lewis 2016, Skeie *et al* 2018, see Knutti *et al* 2017 for a comprehensive summary). Deriving observational constraints on the effective climate sensitivity (S_{hist}) from the historical period is challenging due to the uncertainties in radiative forcing, ocean warming, and the role of internal climate variability in long-term change (Gregory *et al* 2002, Otto *et al* 2013, Forster 2016). The resulting S_{hist} estimates are subject to assumptions about radiative forcing, which are strongly affected by uncertainty in the forcing by anthropogenic aerosols. Also, the observed warming estimates are subject to incomplete coverage, which is especially low in the earlier historical period (Cowtan and Way 2014). In addition, fitting simple climate models to observations as done in Aldrin *et al* (2012) and Johansson *et al* (2015), for example, is subject to uncertainty in those simple models and can be quite sensitive to assumptions (see discussion in Sherwood *et al* in review).

The uncertainty arising from the unknown magnitude of the aerosol forcing in the historical period could be avoided by focusing on the observed warming that has been attributed to greenhouse gases only. Few previous studies (Frame *et al* 2005, Lewis 2016) followed that idea and derived constraints on the effective climate sensitivity by making use of the anthropogenic or greenhouse gas attributable warming, obtained in a detection and attribution analysis. However, these studies did not obtain greenhouse gas attributable ocean heat content in a detection and attribution analysis, using instead the observed ocean heat content estimates to all forcing.

Here, we make use of detection and attribution techniques to quantify both the greenhouse gas attributable change in surface temperature (using blended surface air and sea surface temperature, for a direct comparison with the observed warming), and ocean heat content. We then apply those results to the planetary energy budget using the forcing-feedback framework (Gregory *et al* 2004, Otto *et al* 2013) to derive observational constraints on the effective climate sensitivity ($S_{hist_{GHG}}$). These results are then compared with an alternative approach of applying observational constraints on future model projections.

2. Methods

2.1. Greenhouse gas attributable warming and ocean heat content

To derive the greenhouse gas attributable contributions to the ocean heat content (ΔN_{GHG}) and to temperature (ΔT_{GHG}) we make use of detection and attribution method of regularised optimal fingerprinting (ROF; Ribes and Terray 2013, Ribes *et al* 2013), which is based on a total least squares regression (Allen and Stott 2003). Under the assumption of linear additivity of the forcings (e.g. Hegerl *et al* 1997, Tett *et al* 1999, Gillett *et al* 2004, Swart *et al* 2018), the true observed climate response (y^*) can be expressed as a sum of the models' noise-free responses to individual forcings (x^*_i), scaled by respective scaling factors (β_i) (equation (1)). This method accounts for noise due to internal variability in observations ε_y, and noise $\varepsilon_{x,\,i}$ in the model response due to internal variability and a finite ensemble size for each noise-free modelled response (x^*_i) (Ribes *et al* 2013):

$$y^* = \sum_{i=1}^{l} \beta_i x_i^* \qquad (1)$$

The scaling factors (β_{GHG}) for the ocean warming were derived in the same way as in Tokarska *et al* (2019) (based on the period 1955–2012, due to available observational coverage), for the set of models considered here (supplementary table S1, available online at stacks.iop.org/ERL/15/034043/mmedia). The scaling factors for surface warming were derived using the models' surface warming as a blended product of surface air temperature and the sea surface temperatures, for consistency with the observations (HadCRUT4.5; Morice *et al* 2012), as in Schurer *et al* (2018), following Cowtan *et al* 2015, for the period 1862–2012. In both cases (for ocean warming and surface warming), the models' responses were calculated in the same way as observations, and masked according to the observational coverage at each time step, to allow for a like-to-like comparison of models and observations, prior to the detection and attribution. Prior to masking, model output was re-gridded by bilinear interpolation onto the respective observational grids, and on the common depth layers (in case of ocean warming). In the energy budget analysis that follows in the results section (section 3.3), we make use of full coverage of model simulated responses in
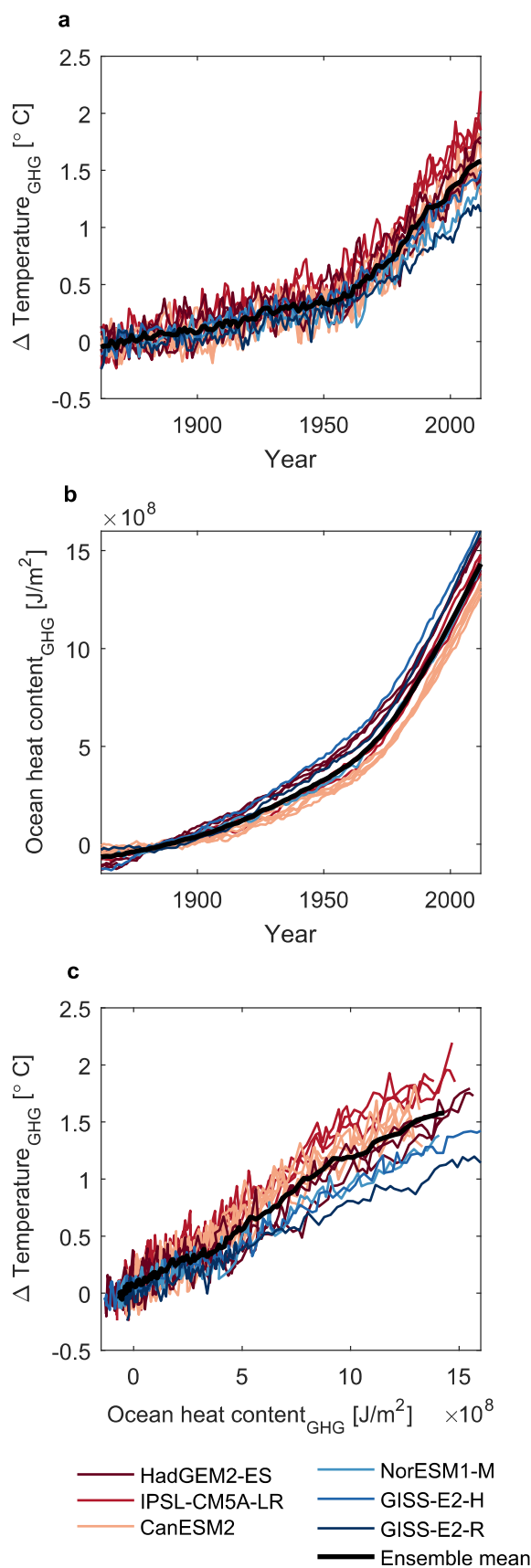
Figure 1. Time-series of model responses to greenhouse gas forcing: surface temperature (a), and ocean heat uptake at 0–2000 m (b). Panel (c) shows the relationship between the top two panels: surface air temperature as a function of ocean heat content (in response to greenhouse gas forcing alone). *Note: All panels show responses to greenhouse gas only (GHG) forcing, based on CMIP5 models (as labelled) in historical GHG-only simulations. Higher ECS models are indicated by red, while lower ECS models are indicated in blue (supplementary table S1). Surface air temperature is shown with respect to the 1862–1880 period.*

greenhouse gas only historical simulations in order to avoid low bias due to missing values (Benestad *et al* 2019), multiplying the model simulated space-time patterns by the range of the β_{GHG} scaling factors that are consistent with observed changes.

We carried on the detection and attribution (ROF) analysis on different sets of inputs, summarised in supplementary table S2. (The detection and attribution analysis is described in detail in Tokarska *et al* (2019) and follows the Ribes *et al* (2013) approach.) We use also historical simulations driven by natural-only and greenhouse gas-only forcings that extend to the year 2012. The historical all-forcing simulations were obtained either using the extensions (until the year 2012) or extended by the first few years from RCP 4.5 simulations (for the period 2006–2012).

Internal variability is considered in detection and attribution, and its effect is included in the uncertainty ranges of the scaling factors. In order to estimate the sensitivity of results to uncertainty in estimates of internal variability we also use detection and attribution results where the noise due to internal variability was doubled by increasing the variance (in the noise from the control runs) by a factor of two (as in Tokarska *et al* 2019).

2.2. Greenhouse gas attributable effective climate sensitivity ($S_{hist_{GHG}}$)

The ECS is determined by atmospheric feedbacks to increases in greenhouse gases, (see definition above). In models, it is usually derived from simulations of greenhouse warming at equilibrium or in response to a large abrupt forcing (i.e. high signal-to-noise ratio; Marvel *et al* 2018). It has been recognised that the feedbacks to an early and increasing warming of the climate system in response to increasing greenhouse gases may not be identical to those to equilibrated greenhouse warming. Also, feedbacks are influenced by spatial patterns of warming (Knutti *et al* 2017, Andrews *et al* 2018), which means that the effective climate sensitivity during the historical period may be different from that at equilibrium. Therefore, if derived from the historical period, ECS is referred to as the *effective* climate sensitivity (Gregory *et al* 2004, Otto *et al* 2013, Forster 2016), and can be expressed as S_{hist} in equation (2):

$$S_{hist} = \frac{F_{2\times CO_2}\Delta T}{\Delta F - \Delta N}, \qquad (2)$$

where $F_{2\times CO_2}$ is the radiative forcing to CO_2 doubling (quantified in a standard 1% per year CO_2 increase experiment), ΔT is warming in the given historical period, ΔF is the radiative forcing estimate, and ΔN is the net energy imbalance, dominated by the ocean heat uptake (Rhein *et al* 2013). S_{hist} in equation (2) is equal to the ECS only if the feedbacks that determine it (often characterised by a parameter in an energy budget equation) are the same at present as at equilibrium.

This energy budget considers the total effective radiative forcing over the historical period, whose largest uncertainty is due to the uncertainty of aerosol forcing: aerosols cause cooling, which may mask out some of the warming caused by greenhouse gases. Here we aim to avoid aerosol uncertainty by making use of the atmospheric and ocean warming that has been attributed to greenhouse gases alone (dominated by CO_2 radiative forcing). Hence, based on equation (2), we define the effective climate sensitivity due to greenhouse gas-attributable response as $S_{hist_{GHG}}$, expressed by equation (3):

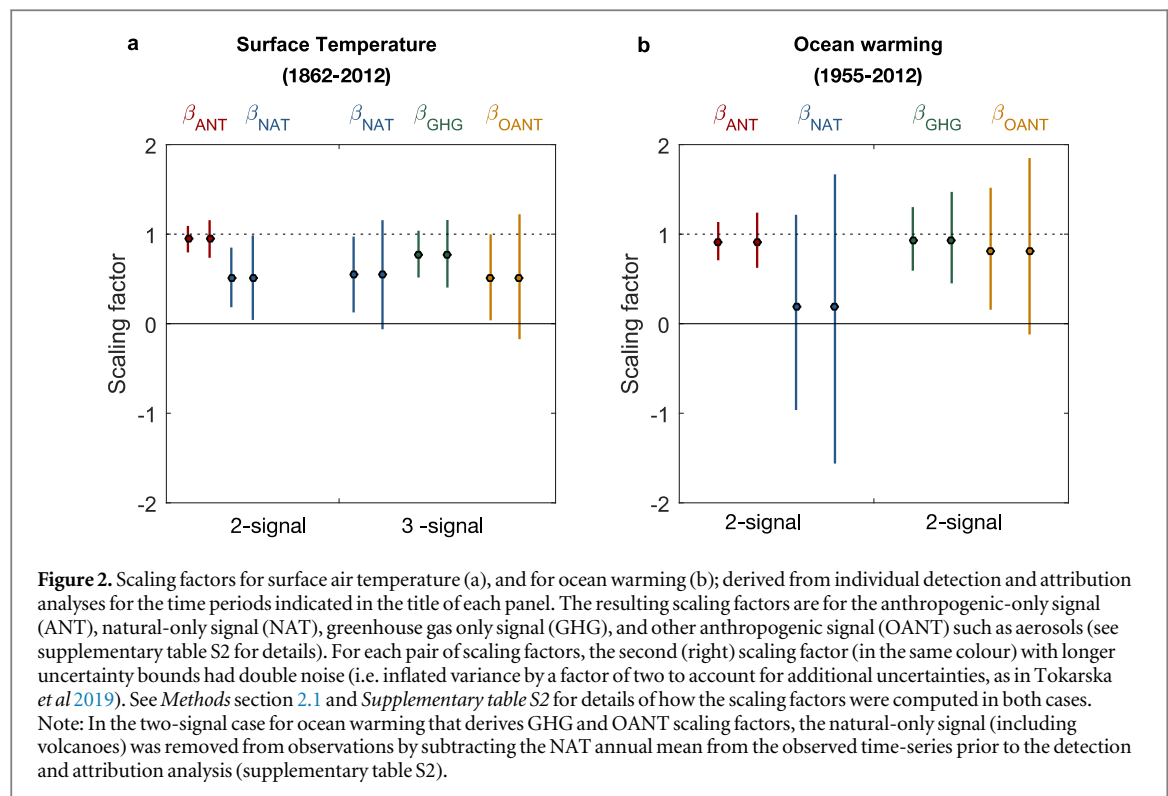$$S_{hist_{GHG}} = \frac{F_{2\times CO_2}\Delta T_{GHG}}{\Delta F_{GHG} - \Delta N_{GHG}}, \qquad (3)$$

where ΔF_{GHG} is the greenhouse gas effective radiative forcing for the analysis period. Both the greenhouse gas attributable warming (ΔT_{GHG}) and the greenhouse gas attributable ocean heat content change (ΔN_{GHG}, representing the net energy imbalance) and their respective uncertainties in the greenhouse gas attributable responses are obtained by scaling the model responses in surface air temperature and ocean heat content by the corresponding scaling factors β_{GHG} derived in a detection and attribution analysis (see section 2.1 and supplementary tables S2 and S3).

In section 3.3, we compute probability density distributions of $S_{hist_{GHG}}$ in two following ways. First, we calculated $S_{hist_{GHG}}$ directly by drawing random samples from Gaussian distributions (or joined half-Gaussian, if the 5%–95% attributed range was not symmetric; supplementary figure S1) of all the parameters on RHS of equation (3). (See Supplementary tables S1 to S4 for details, and supplementary figure S1 illustrating the input distributions.) The spread for of ΔT_{GHG} comes from the uncertainty range in the β_{GHG} scaling factors times the model simulated change, replicating the fit to observations (figure 2). However, this direct approach of obtaining $S_{hist_{GHG}}$ is subject to an implicit prior on $S_{hist_{GHG}}$ which may be biasing the distribution towards lower $S_{hist_{GHG}}$ values by under-sampling high S_{hist} values (Frame *et al* 2005).

To evaluate the implications of such an implicit prior on $S_{hist_{GHG}}$, we also took an alternative approach (Sherwood *et al* in review), where we assume a flat uniform prior on $S_{hist_{GHG}}$ and then calculated the expected warming $\Delta T_{exp_{GHG}}$ given the ranges of ΔF_{GHG}, ΔN_{GHG}, and $F_{2\times CO_2}$, by re-arranging equation (3) into a forward model. For a putative value of $S_{hist_{GHG}}$, the expected temperature is:

$$\Delta T_{exp_{GHG}} = S_{hist_{GHG}}\frac{\Delta F_{GHG} - \Delta N_{GHG}}{F_{2\times CO_2}} + \varepsilon, \qquad (4)$$

where ε is the observational error (including observational uncertainty and unforced climate variability (Sherwood *et al* in review). As before, the inputs ΔF_{GHG}, ΔN_{GHG}, and $F_{2\times CO_2}$ are sampled from corresponding Gaussian or joined half-Gaussian (if not symmetric) distributions using the random sampling approach (i.e. drawing random samples from the

Figure 2. Scaling factors for surface air temperature (a), and for ocean warming (b); derived from individual detection and attribution analyses for the time periods indicated in the title of each panel. The resulting scaling factors are for the anthropogenic-only signal (ANT), natural-only signal (NAT), greenhouse gas only signal (GHG), and other anthropogenic signal (OANT) such as aerosols (see supplementary table S2 for details). For each pair of scaling factors, the second (right) scaling factor (in the same colour) with longer uncertainty bounds had double noise (i.e. inflated variance by a factor of two to account for additional uncertainties, as in Tokarska *et al* 2019). See *Methods* section 2.1 and *Supplementary table S2* for details of how the scaling factors were computed in both cases. Note: In the two-signal case for ocean warming that derives GHG and OANT scaling factors, the natural-only signal (including volcanoes) was removed from observations by subtracting the NAT annual mean from the observed time-series prior to the detection and attribution analysis (supplementary table S2).

input distributions), but $\Delta T_{exp_{GHG}}$ in equation (4) is evaluated for $S_{hist_{GHG}}$ values ranging from 0 to 10 K, sampling a uniform prior. (We also performed sensitivity to the choice of a different range of the prior 0 °C to 5 °C, and 0 °C to 20 °C, which does not influence our results to first decimal place).

The resulting expected warming ($\Delta T_{exp_{GHG}}$) can be then evaluated against the observationally-constrained greenhouse gas attributable warming ($\Delta T_{OBS_{GHG}}$), allowing us to derive the likelihood of $S_{hist_{GHG}}$, and its corresponding posterior probability density. The likelihood of $S_{hist_{GHG}}$ is calculated by evaluating the distance for each of the random samples of expected warming ($\Delta T_{exp_{GHG}}$) to the greenhouse gas attributable warming ($\Delta T_{OBS_{GHG}}$). To avoid summing extremely low density values, we considered only density values which fall within 3σ of the mean value of $\Delta T_{exp_{GHG}}$, which were then aggregated for each corresponding $S_{hist_{GHG}}$ value, resulting in the likelihood distribution for S_{GHG}.

This likelihood $P(T_{OBS_{GHG}} | S_{hist_{GHG}}, \Delta N_{GHG}, \Delta F_{GHG}, \Delta F_{2 \times CO_2})$ quantifies how likely the observation-based greenhouse gas attributable warming $\Delta T_{OBS_{GHG}}$ would be, given the expected ranges of ΔF_{GHG}, ΔN_{GHG}, and $F_{2 \times CO_2}$ and considering all plausible values of $S_{hist_{GHG}}$ (expressed by the flat prior) (as in Sherwood *et al* in review). Since the prior $S_{hist_{GHG}}$ distribution $P(S_{hist_{GHG}})$ is represented by a flat prior, the posterior distribution $P(S_{hist_{GHG}} | T_{OBS_{GHG}}, \Delta N_{GHG}, \Delta F_{GHG}, \Delta F_{2 \times CO_2})$ is then the likelihood distribution normalised to a unit area. Supplementary table S3 contains the values of parameters used in the two different distributions discussed in section 3.3.

3. Results

3.1. Surface air temperature and ocean heat content in GHG-only simulations

Both surface air temperature and ocean heat content continually increase in the historical period in response to greenhouse gas forcing in historical greenhouse gas only simulations (figures 1(a), (b)). As a result, there is an approximately linear relationship between the greenhouse gas attributable temperature and ocean heat content, shown in figure 1(c). We make use of this emergent property of the climate system in response to greenhouse gases alone later in section 3.4 to provide observational constraints on the historical greenhouse gas attributable responses. (Note that models with high atmospheric warming do not necessarily have larger increases in ocean heat content, for the periods considered here.)

3.2. Adjustments to greenhouse gas attributable responses

To derive the observationally-constrained greenhouse gas attributable surface air temperature and ocean warming, we performed a detection and attribution analysis (Methods section 2.1). The resulting scaling factors (figure 2) were derived separately for the surface air warming (based on HadCRUT4.5 observations) and ocean warming (based on the Levitus *et al* 2012 dataset, and following the methodology in Tokarska *et al* 2019), as specified in Supplementary table S4. In the detection and attribution analysis (following Ribes *et al* 2013 and Tokarska *et al* 2019), the scaling factors were obtained by regressing the

observations onto model response patterns (Methods section 2.1; supplementary table S2). The scaling factors and their uncertainty range resulting from the attribution analysis indicate how much the modelled response to each forcing needs to and can be adjusted to reconstruct the observations (Methods, section 2.1).

Our results show that for both, surface air warming (in the 1861–2012 period) and ocean warming (in the 1955–2012 period), the best estimate greenhouse gas only response is well constrained and can be separated from natural and other anthropogenic responses for surface temperature (figure 2), and from other anthropogenic factors for ocean warming, with natural forcing estimated to have only a small influence (see Tokarska *et al* 2019). The greenhouse gas response is found to be slightly smaller in the multi-model mean than in observations, and thus is adjusted slightly downward (β_{GHG} scaling factors less than 1; figure 2), but this adjustment is not significant (error bars consistent with no adjustment, i.e. scaling factor consistent with 1; figure 2). Next, we make use of the β_{GHG} scaling factors, applied to the greenhouse gas only time-series (figure 1), to calculate the observationally-constrained greenhouse gas attributable responses for the historical period (supplementary tables S2, S3), and the resulting effective climate sensitivity $S_{hist_{GHG}}$, in section 3.3. Note that figure 2 shows for comparison also scaling factors for anthropogenic combined warming which are not used in this study, but they show that the attribution results are robust between signal combinations.

3.3. Energy budget approach to the greenhouse gas attributable effective climate sensitivity

The greenhouse gas-attributable responses (figure 1), scaled by the respective β_{GHG} scaling factors to better match the observations (figure 2; Methods section 2.1), allow us to derive a probability distribution for the observationally-constrained, greenhouse gas attributable, effective climate sensitivity $S_{hist_{GHG}}$. We make use of the energy budget equation (equation (2)), using the following two approaches: (1) a direct sampling approach (Methods, equation (3)), and a 'forward model' approach (Methods, equation (4); flat prior in $S_{hist_{GHG}}$).

We carried on analysis on two different periods: 1862–2012 (Case A) and for 1955–2012 (Case B), with inputs described in supplementary table S3. In this section, case names with number '1' (i.e. A1, B1) have regular noise, and case names with number '2' (i.e. A2, B2) have doubled the noise (by doubling the variance obtained in the control-run simulations) prior to detection and attribution. Such inflating of the noise results in wider uncertainty ranges of the scaling factors, and wider overall uncertainty ranges. This factor has been estimated as approximately correcting for the uncertainty of using the multi-model mean response

instead of fully accounting for climate model response pattern uncertainty (Schurer *et al* 2018).

We assume that the scaling factors β_{GHG}, which describe the strength of the modelled response to forcing, are constant through time. We calculate the scaling factors for surface temperature and ocean heat content using the longest period available (as in figure 2). We then apply those scaling factors to the two different time periods: 1862–2012 (case A), and 1955–2012 (case B). Specifically, the scaling factor β_{GHG} ocean heat content was derived for the period 1955–2012 only, as earlier observations are not available, and is applied to ocean heat content changes in climate models across the full analysis period time periods in each case (case A that covers 1862–2012 period, and case B that covers 1955–2012 period). Similarly, the scaling factor β_{GHG} for surface air temperature was derived for the period with longest observational data available (i.e. 1862–2012), and is applied in both cases A and B of the analysis here.

The resulting probability distributions from random sampling of the observationally-constrained greenhouse gas attributable responses (Methods, section 2.2), yield an estimate of the greenhouse gas attributable effective climate sensitivity ($S_{hist_{GHG}}$) for the period 1862–2012 (case A) that ranges from 1.3 °C to 3.1 °C (5%–95% interval with the most likely value at 1.9 °C, and median of 2.0 °C ; figure 3; 'Box model' case A1) using the direct sampling approach, and from 1.3 to 3.1 °C (5%–95% interval with the most likely value at 2.0 °C, and median 2.1 °C; figure 3(a); 'Forward model' case A1). Using the 'forward model' approach which is based on an explicit flat prior on ECS hence shows only small sensitivity to the prior information used (supplementary table S4). However, using the a different period 1955–2012 (case B) results in higher values of $S_{hist_{GHG}}$, with the median 2.8 °C, most likely value 2.6 °C, and the 5%–95% range of 1.7 °C–4.6 °C (figure 3(b); case B1 Box model, supplementary table S4). The uncertainty bounds are wider in case B, compared to case A, showing that the observational constraint from the shorter period is weaker. Using the longer period also results in better constrained greenhouse gas attributable warming. Using double-noise in β_{GHG} factors (figure 2), and sampling from the resulting inflated Gaussian distribution yields $S_{hist_{GHG}}$ that also have wider uncertainty bounds (Cases A2, B2, figure 3, supplementary table S3 and S4).

Our estimate of $S_{hist_{GHG}}$ is lower than the documented ECS of some climate models (e.g. CMIP5 multi-model mean ECS of 3.22 °C; Forster *et al* 2013), including that of some used in the analysis (see supplementary table S1). However, it is well understood that time-dependent feedbacks might render $S_{hist_{GHG}}$ lower than S at equilibrium (Knutti *et al* 2017, Andrews *et al* 2018). Furthermore, different ways of calculating ECS in climate models results in different values, which are
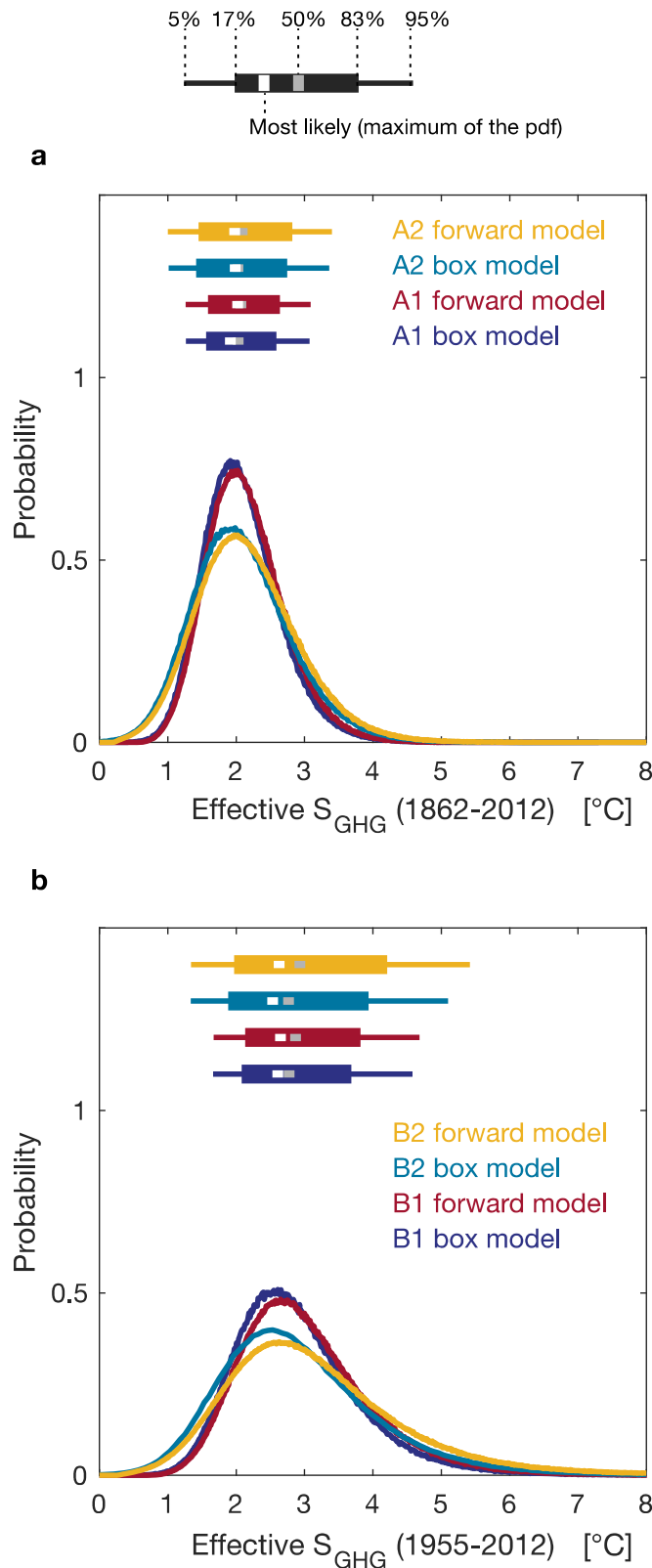
Figure 3. Probability distributions of the greenhouse gas attributable effective climate sensitivity ($S_{histGHG}$), using the direct sampling approach and the forward model approach. (a) Cases A: for the period 1862–2012; (b) cases B: for the period 1955–2012, with scaling factors as in panel (a). Light blue and yellow lines (cases A2, B2) were derived in the same way as the cases A1, B1 but include results with double noise (i.e. wider uncertainty in the input parameters due to wider uncertainty on β_{GHG}). Bars on the right panel indicate the most likely and median values with the likely (17%–83%) and 5%–95% confidence intervals, for each distribution, as labelled. For description of each case and more detail, see supplementary tables S3 and S4. The energy budget (equation (2)) has been applied to the period 1862–2012 (panel (a)), and 1955–2012 in panel (b). β_{GHG} to scale the ocean heat content was derived for the period 1955–2012 in both cases, and β_{GHG} to scale temperature derived for the period 1862–2012 in both cases (see section 3.2).

often lower than the true ECS when using equilibrated simulations (Rugenstein *et al* 2019).

Such lower values for $S_{hist_{GHG}}$ than S at equilibrium can be explained by the effects of changing strength of the feedbacks at higher levels of warming (Knutti *et al* 2017). The climate feedback parameter (defined as $1/S_{hist}$) has been shown to vary in the historical period (Gregory and Andrews 2016, Andrews *et al* 2018), and depends on both time-variation and the forcing agent. Andrews *et al* 2018 show that the feedback parameter ($1/S_{hist}$) is decreasing, particularly after 1940s onwards (Andrews *et al* 2018; figure 2(f) therein). This would suggest increase in S_{hist} during that period. Potential changes in feedbacks are neglected if assuming that S_{hist} is equal to S (at equilibrium), an assumption often made if inferring S using simple climate models with constant feedbacks. Our tighter and lower values for $S_{hist_{GHG}}$ may be affected by this effect, but may alternatively also reflect better constraints with a longer time horizon, or be affected by uncertainties in the early record we can not fully quantify. For example, an uncertainty in the long period is that it effectively uses extrapolation of the observational constraint from the second half of the 20th century to the full analysis period, which may introduce error particularly if some model simulations are affected by drift in the ocean. Also, analysis periods can matter both due to effects of internal climate variability and possibly residuals from responses by other forcings that may have been not fully separated in the attribution analysis.

The increased greenhouse gas scaling factors, and with it the increase in estimated effective climate sensitivity calculated from the recent period (1955–2012) could reflect feedbacks associated with a rapid increase in greenhouse gas forcing. Gregory *et al* (2019) also find that the effective climate sensitivity is higher since the year 1975 when greenhouse gas forcing has rapidly increased. Alternative approaches have been also suggested to this simple energy balance model (equation (2)) that account for stratospheric adjustments, which are related to the changing feedback parameters (Ceppi and Gregory 2019).

3.4. Observational constraints on the climate model responses

In this section we use the attributed greenhouse warming in atmosphere and ocean to directly evaluate the model simulated greenhouse gas response. This is to address the problem that time-dependent feedbacks might render $S_{hist_{GHG}}$ lower than S at equilibrium, as discussed above section 3.3. The analysis presented here allows us also to evaluate if the rate of heat entering the ocean instead of warming the atmosphere is correct in models. There could be a trade-off between ocean warming and surface warming (for example, some climate models may be very sensitive and show too high ECS, yet mix heat rapidly into the

ocean over the historical period, resulting in surface warming that resembles observations). In order to evaluate if such a trade-off exists, we plotted the greenhouse gas attributable surface temperature change (i.e. greenhouse gas only multi-model mean scaled by the β_{GHG} scaling factor that results in an observationally-constrained quantity) against the greenhouse gas attributable ocean heat content (also multi-model mean scaled by the respective β_{GHG}), which serve as an observational constraint. We then compare these observationally-constrained ranges with each ensemble member of the historical greenhouse gas only simulation for the models considered here. The observed attributable trend was arrived at by adjusting the multi-model mean from CMIP5 models considered here (figure 4; black empty diamond) by β_{GHG} factors (for ocean and surface air temperature, respectively, as in figure 2), and is shown as the black full diamond. Grey rectangles indicate uncertainty range based on β_{GHG} scaling factors given model internal variability noise (smaller square), and doubled noise in input parameters (larger square; Methods section 2.1). For simplicity, we assume no dependence between ocean and atmospheric warming estimates (note that as the corners of the rectangles are not populated in our examples, this simplification is not important here).

If a model's true forced signal (i.e. its well estimated ensemble mean) falls within the grey rectangles, such model's greenhouse gas response in both ocean and atmosphere is considered to be consistent with the observed greenhouse gas attributable surface air and ocean warming individually. Based on this simple selection, our results suggest that almost all climate models considered here are within the observationally-constrained greenhouse gas attributable ocean warming. Figure 4 also shows that the models spread in their simulated surface air and ocean warming in response to greenhouse gas forcing, but there is no indication of a correlation of points across the two axes, suggesting that the independent treatment of both constraints here is reasonable, and that there are no models that hide strong sensitivity through stronger ocean warming or that show weak warming compensated by lack of ocean heat uptake. Of the three models with ECS values outside our $S_{hist_{GHG}}$ values (3.4 °C as the 95th percentile in A2 forward model case, figure 3(a); for the longer analysis period 1862–2012), indicated in red in figure 4(a) (see supplementary table S1 for climate sensitivity values), two are clearly consistent with the observed greenhouse gas signal in atmosphere and ocean in figure 4 (i.e. are within the grey rectangle), emphasising the importance of changing feedbacks with time in these models. In the case of one model with climate sensitivity exceeding 4 °C, however, all individual greenhouse gas simulations are outside even the narrower grey rectangle, suggesting that this model warms too much in surface temperature to be consistent with the
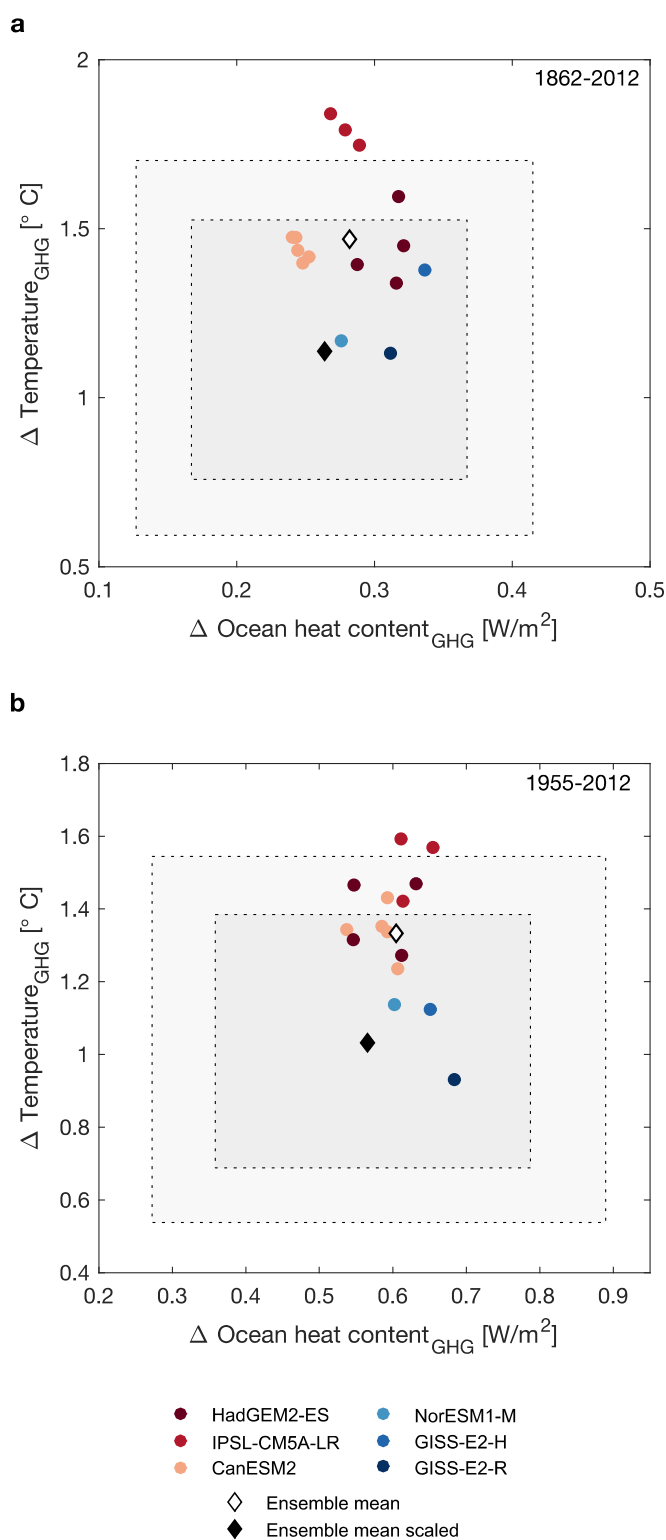
Figure 4. Greenhouse gas-only surface temperature change as a function of greenhouse gas-only ocean heat content change. (a) For the period 1862–2012, as in case A; (b) for the period 1955–2012, as in case B (see supplementary table S3 for details). The empty black diamond indicates the multi-model mean from CMIP5 models considered here, while the full black diamond indicates the adjusted multi-model CMIP5 mean, scaled by β_{GHG} factors (i.e. observationally-constrained greenhouse gas attributable response for ocean heat content and surface air temperature, respectively, as in figure 2). The grey rectangles indicate the uncertainty range from those observation-constrained scaling factors (figure 2) with regular noise (darker grey rectangle) and double noise (light grey rectangle). Symbols of the same colour indicate individual ensemble members of the same model. Higher ECS models are indicated by red, while lower ECS models are indicated in blue (supplementary table S1). See supplementary tables S3 and S4 for details.

attributed greenhouse gas warming. Figure 4 illustrates that the multi-model-ensemble mean in response to greenhouse gas forcing is encompassed by the observationally-constrained rectangles.

3.5. Sources of uncertainty

The detection and attribution analysis used in this study assumes linear additivity of the forcings, which has been shown to be a reasonable assumption both for surface warming (Hegerl *et al* 1997, Tett *et al* 1999, Gillett *et al* 2004), and ocean warming (Swart *et al* 2018). Also, since we make use of the multi-model mean in the inputs for the detection and attribution, our resulting scaling factors may be over-confident (Schurer *et al* 2018). We have addressed this, at least to some extent, by doubling the noise due to internal variability in preindustrial control simulations that are used for the noise estimate (prior to detection and attribution; as in Schurer *et al* 2018), which resulted in wider uncertainty ranges on the scaling factors (figure 2, see Tokarska *et al* 2019 for more detail) that translate to wider uncertainty ranges in the input Gaussian distributions (supplementary figures S1 and S2). Since fewer models are used in this analysis than in Tokarska *et al* 2019, the scaling factors β_{GHG} for the ocean have larger uncertainty bounds than if using more models.

Assumptions about the priors are crucial in probabilistic estimates of climate sensitivity (Frame *et al* 2005), and our choice of parameters is indicated in Supplementary table S3. For simplicity, in the energy budget equation (equation (3)), we assume that all the heat storage occurs in the ocean (ΔN_{GHG} component), as the ocean dominates the planetary heat storage (Rhein *et al* 2013), and is based only on the top 2000 m of ocean depths. Taking these two assumptions into account (land heat storage contribution and CO_2 co-depended in radiative forcing terms) does not have much impact on the resulting ECS likelihood distribution (Sherwood *et al* in review). Also, we did not separate the CO_2 radiative forcing contributions in the $F_{2 \times CO_2}$ and ΔF_{GHG} components, thereby assuming that they are independent, though CO_2 is a component of the greenhouse gas forcing radiative forcing ΔF_{GHG}.

4. Discussion and conclusions

A simple zero-dimensional energy balance model (equation (2)) provides a straightforward way of estimating the historical and present-day effective climate sensitivity (S_{hist}) by sampling observed quantities, such as surface air warming and ocean heat content, within their uncertainty range. By sampling greenhouse gas attributable observed quantities, we provide an observational constraint on climate sensitivity $S_{hist_{GHG}}$ as driven by feedbacks over the historical period, which is not subject to uncertainties in the aerosol forcing. This output distribution of $S_{hist_{GHG}}$ is only slightly sensitive to using a flat prior in S versus directly sampling from the input distributions (i.e. differences between the direct sampling approach 'Box model' and the 'Forward model' approach), and also widens only slightly if considering larger observational uncertainties (i.e. doubling the noise due to internal variability prior to detection and attribution analysis; supplementary figures S1 and S2).

Recently, Tokarska *et al* (2020) found that the recent historical period can provide an observational constraint on simulated warming rates in the future, and that some models with high climate sensitivities are not consistent with the observed warming trends for the recent decades. The approach presented here finds only a weak observational constraint, with only one model being outside the observationally-constrained range, and a few models being close to the edge, suggesting that the greenhouse gas observationally-constrained response is not presently a strong constraint for the future, despite suggesting a narrower range of $S_{hist_{GHG}}$ than supported by some models. However, uncertainties considered here are different in this approach, with more explicit consideration of uncertainty due to natural forcing and uncertainty in the aerosol forcing, at the cost of a weaker result (i.e. the observationally-constrained range here ends up being wider, thus screening-in more models). Also, the time-period considered here is different, and ends sooner than those considered by Tokarska *et al* (2020).

Our results also suggest that the true ECS is likely to be higher than the effective climate sensitivity inferred from historical observations. We emphasise that dimensions other than global mean temperature rise need to be taken into account when discussing either past or future climate change. Increases in greenhouse gases also lead to changes in other components of the climate system, such as hydrological cycle and carbon cycle changes that may not necessarily scale linearly with the global mean temperature rise.

Diagnosis and Intercomparison provides coordinating support and led development of software infrastructure in partnership with the Global Organization for Earth System Science Portals.

Data statement

Data used in this study is available from the following sources:

CMIP model output is available at: http://pcmdi9.llnl.gov/.

Ocean warming data is available at: https://nodc.noaa.gov/OC5/3M_HEAT_CONTENT/.

Blended-masked HadCRUT4 time-series are available from the corresponding author upon request.

The Regularised Optimal Fingerprinting (ROF) detection and attribution package developed by Aurélien Ribes is available at https://umr-cnrm.fr/spip.php?article23&lang=fr.

ORCID iDs

Katarzyna B Tokarska https://orcid.org/0000-0001-8887-8798
Gabriele C Hegerl https://orcid.org/0000-0002-4159-1295
Andrew P Schurer https://orcid.org/0000-0002-9176-3622

References

Aldrin M, Holden M, Guttorp P, Skeie R B, Myhre G and Berntsen T K 2012 Bayesian estimation of climate sensitivity based on a simple climate model fitted to observations of hemispheric temperatures and global ocean heat content *Environmetrics* **23** 253–71

Allen M R and Stott P A 2003 Estimating signal amplitudes in optimal fingerprinting: I. Theory *Clim. Dyn.* **21** 477–91

Andrews T, Gregory J M, Paynter D, Silvers L G, Zhou C, Mauritsen T, Webb M J, Armour K C, Forster P M and Titchner H 2018 Accounting for changing temperature patterns increases historical estimates of climate sensitivity *Geophys. Res. Lett.* **45** 8490–9

Benestad R E, Erlandsen H B, Mezghani A and Parding K M 2019 Geographical distribution of thermometers gives the appearance of lower historical global warming *Geophys. Res. Lett.* **46** 7654–62

Ceppi P and Gregory J M 2019 A refined model for the Earth's global energy balance *Clim. Dyn.* **53** 4781–97

Church J A *et al* 2013 Sea level change *Climate Change 2013: The Physical Science Basis. Contribution of Working Group I to the Fifth Assessment Report of the Intergovernmental Panel on Climate Change* ed T F Stocker *et al* (Cambridge and New York: Cambridge University Press)

Cowtan K, Hausfather Z, Hawkins E, Jacobs P, Mann M E, Miller S K, Steinman B A, Stolpe M B and Way R G 2015 Robust comparison of climate models with observations using blended land air and ocean sea surface temperatures *Geophys. Res. Lett.* **42** 6526–34

Cowtan K and Way R G 2014 Coverage bias in the HadCRUT4 temperature series and its impact on recent temperature trends *Q. J. R. Meteorol. Soc.* **140** 1935–44

Dessler A E and Forster P M 2018 An estimate of equilibrium climate sensitivity from interannual variability *J. Geophys. Res.: Atmos.* **123** 8634–45

Forster P M *et al* 2013 Evaluating adjusted forcing and model spread for historical and future scenarios in the CMIP5 generation of climate models *J. Geophys. Res.: Atmos.* **118** 1139–50

Forster P M 2016 Inference of climate sensitivity from analysis of Earth's energy budget *Annu. Rev. Earth Planet. Sci.* **44** 85–106

Frame D J, Booth B B B, Kettleborough J A, Stainforth D A, Gregory J M, Collins M and Allen M R 2005 Constraining climate forecasts: the role of prior assumptions *Geophys. Res. Lett.* **32** L09702

Gillett N P, Wehner M F, Tett S F B and Weaver A J 2004 Testing the linearity of the response to combined greenhouse gas and sulfate aerosol forcing *Geophys. Res. Lett.* **31** L14201

Gregory J M and Andrews T 2016 Variation in climate sensitivity and feedback parameters during the historical period *Geophys. Res. Lett.* **43** 3911–20

Gregory J M, Andrews T, Ceppi P, Mauritsen T and Webb M J 2019 How accurately can the climate sensitivity to CO_2 Be estimated from historical climate change? *Clim. Dyn.* **54** 129–57

Gregory J M, Ingram W J, Palmer M A, Jones G S, Stott P A, Thorpe R B, Lowe J A, Johns T C and Williams K D 2004 A new method for diagnosing radiative forcing and climate sensitivity *Geophys. Res. Lett.* **31** L03205

Gregory J M, Stouffer R J, Raper S C B, Stott P A and Rayner N A 2002 An observationally based estimate of the climate sensitivity *J. Clim.* **15** 3117–21

Hansen J, Sato M, Kharecha P and von Schuckmann K 2011 Earth's energy imbalance and implications *Atmos. Chem. Phys.* **11** 13421–49

Harris G R, Sexton D M H, Booth B B B, Collins M and Murphy J M 2013 Probabilistic projections of transient climate change *Clim. Dyn.* **40** 2937–72

Hegerl G C, Hasselmann K, Cubasch U, Mitchell J F B, Roeckner E, Voss R and Waszkewitz J 1997 Multi-fingerprint detection and attribution analysis of greenhouse gas, greenhouse gas-plus-aerosol and solar forced climate change *Clim. Dyn.* **13** 613–34

Johansson D J A, O'Neill B C, Tebaldi C and Häggström O 2015 Equilibrium climate sensitivity in light of observations over the warming hiatus *Nat. Clim. Change* **5** 449–53

Knutti R, Rugenstein M A A and Hegerl G C 2017 Beyond equilibrium climate sensitivity *Nat. Geosci.* **10** 727–36

Levitus S *et al* 2012 World ocean heat content and thermosteric sea level change (0–2000 m), 1955–2010 *Geophys. Res. Lett.* **39** L10603

Lewis N 2016 Implications of recent multimodel attribution studies for climate sensitivity *Clim. Dyn.* **46** 1387–96

Marvel K, Pincus R, Schmidt G A and Miller R L 2018 Internal variability and disequilibrium confound estimates of climate sensitivity from observations *Geophys. Res. Lett.* **45** 1595–601

Millar R J *et al* 2015 Model structure in observational constraints on transient climate response *Clim. Change* **131** 199–211

Morice C P, Kennedy J J, Rayner N A and Jones P D 2012 Quantifying uncertainties in global and regional temperature change using an ensemble of observational estimates: the HadCRUT4 data set *J. Geophys. Res.: Atmos.* **117** D08101

Otto A *et al* 2013 Energy budget constraints on climate response *Nat. Geosci.* **6** 415–6

Rhein M *et al* 2013 Observations: ocean *Climate Change 2013: The Physical Science Basis. Contribution of Working Group I to the Fifth Assessment Report of the Intergovernmental Panel on Climate Change* ed T F Stocker *et al* (Cambridge and New York: Cambridge University Press)

Ribes A, Planton S and Terray L 2013 Application of regularised optimal fingerprinting to attribution. Part I: method, properties and idealised analysis *Clim. Dyn.* **41** 2817–36

Ribes A and Terray L 2013 Application of regularised optimal fingerprinting to attribution. Part II: application to global near-surface temperature *Clim. Dyn.* **41** 2837–53

Rugenstein M *et al* 2019 Equilibrium climate sensitivity estimated by equilibrating climate models *Geophys. Res. Lett.* at press (https://doi.org/10.1029/2019GL083898)

Schurer A, Hegerl G, Ribes A, Polson D, Morice C and Tett S 2018 Estimating the transient climate response from observed warming *J. Clim.* **31** 8645–63

Sherwood S *et al* 2020 A combined assessment of Earth's climate sensitivity *Rev. Geophys.* (in review)

Shindell D T 2014 Inhomogeneous forcing and transient climate sensitivity *Nat. Clim. Change* **4** 274–7

Skeie R B, Berntsen T, Aldrin M, Holden M and Myhre G 2018 Climate sensitivity estimates—sensitivity to radiative forcing time series and observational data *Earth Syst. Dyn.* **9** 879–94

Swart N C, Gille S T, Fyfe J C and Gillett N P 2018 Recent Southern Ocean warming and freshening driven by greenhouse gas emissions and ozone depletion *Nat. Geosci.* **11** 836–41

Tett S F B, Stott P A, Allen M R, Ingram W J and Mitchell J F B 1999 Causes of twentieth-century temperature change near the earth's surface *Nature* **399** 569–72

Tokarska K B, Hegerl G C, Schurer A P, Ribes A and Fasullo J T 2019 Quantifying human contributions to past and future ocean warming and thermosteric sea level rise *Environ. Res. Lett.* **14** 074020

Tokarska K B, Stolpe M B, Sippel S, Fischer E M, Smith C J, Lehner F and Knutti R 2020 Past warming trend constrains future warming in CMIP6 models *Sci. Adv.* at press

van Hateren J H 2013 A fractal climate response function can simulate global average temperature trends of the modern era and the past millennium *Clim. Dyn.* **40** 2651–70

Observational constraints on the effective climate sensitivity

from the historical period

Katarzyna B. Tokarska[1]*, Gabriele C. Hegerl[1], Andrew P. Schurer[1], Piers M. Forster[2], and Kate Marvel[3,4]

[1] School of Geosciences, University of Edinburgh, UK
[2] University of Leeds, UK
[3] NASA Goddard Institute for Space Studies, New York, NY, USA
[4] Department of Applied Physics and Applied Mathematics, Columbia University, New York, NY, USA

* current affiliation: Institute for Atmospheric and Climate Science, ETH Zurich, Zurich, Switzerland

Corresponding author: Katarzyna B. Tokarska (kasia.tokarska@ed.ac.uk)

Supplementary Material

Supplementary Tables S1 to S4.

Supplementary Figure S1 and S2.

Model	Atmosphere	Land	Ocean	ALL forcing	NAT only	GHG only	ECS
HadGEM2-ES	HadGAM2 (N96L38)	TRIFFID	HadGOM2	4	4	4	4.59
IPSL-CM5A-LR	LMDZ	ORCHIDEE	NEMO-OPA	1	3	3	4.13
CanESM2	AGCM4	CLASS	NCAR	5	5	5	3.69
NorESM1-M	CAM4	CLM4	MICOM– HAMOCC	1	1	1	2.8
GISS-E2-H	GISS	GISS	HYCOM	1	1	1	2.31
GISS-E2-R	GISS	GISS	Russell ocean model	1	1	1	2.11
			Total	**14**	**16**	**16**	**3.22** (CMIP5 mean)

Supplementary Table S1. Models and simulations used. The historical simulations for NAT-only and GHG-only historical simulations are until the year 2012. The historical all-forcing simulations were either using the extensions (until the year 2012) or by using the first few years from RCP 4.5 simulations (2006-2012). A full list of the model components and their evaluation can be found in (Sanderson et al. 2015). The climate sensitivity values (ECS) are from (Forster et al., 2013), and CMIP5 mean (in the last row) refers to all CMIP5 modes (not only those shown here), for reference.

Reference:

Forster, P. M. *et al.* Evaluating adjusted forcing and model spread for historical and future scenarios in the CMIP5 generation of climate models. *Journal of Geophysical Research: Atmospheres* **118**, 1139–1150 (2013).

Case name	Input time-series	Output (scaling factors)
Surface warming, 2-signal	ALL, NAT	β_{ANT}, β_{NAT}
Surface warming, 3-signal	ALL, NAT, GHG	$\beta_{GHG}, \beta_{OANT}, \beta_{NAT}$
Ocean warming, 2-signal	ALL ,NAT	β_{ANT}, β_{NAT}
Ocean warming, 2-signal	ANT, GHG, with (OBS -NAT)*	$\beta_{GHG}, \beta_{OANT}$

Acronyms expanded: Anthropogenic-only signal (ANT); natural-only signal (NAT); greenhouse-gas only signal (GHG); other anthropogenic signal (OANT) such as aerosols; observations (OBS);

Supplementary Table S2. Different sets of inputs and outputs for the detection and attribution analysis (Section 2.1 and Section 3.2). ROF analysis on each of the cases was performed twice, where in the second round the variance was inflated to account for additional uncertainties due to internal variability.
Note: In the 2-sginal case for ocean warming that derives GHG and OANT scaling factors, the natural-only signal (including volcanoes) was removed from observations by subtracting the NAT annual mean from the observed time-series prior to the detection and attribution analysis.

Detection and attribution analysis was performed separately for surface warming, and separately for ocean warming, following the regularized optimal fingerprinting method (Ribes et al. 2013).

We make use of all the available ensemble members (listed in Supplementary Table S1), from which we take the multi-model ensemble mean (without calculating ensemble means individually for each model). This ensemble mean was then centered (with the mean for the whole period removed) and divided into 5-year non-overlapping segments, as required by the detection and attribution inputs preparation. For the fingerprints, we make use of global mean and hemispherical contrast for surface warming, and for the ocean warming, we make use of the global mean taken at three representative depth levels at 0-300m, 300-700m, and 700-2000m. In both cases (surface warming and ocean warming), treated individually, the simulated output was re-gridded onto the observational grid and calculated in the same way as the observations. For more details, please see Tokarska et al. 2019, where we discuss how the scaling factors were obtained for ocean warming, and present different sensitivity analyses. For details on the regularized optimal fingerprinting method itself, please see Ribes et al. 2013.

References:
Ribes, A. & Terray, L. Application of regularised optimal fingerprinting to attribution. Part II: application to global near-surface temperature. *Clim Dyn* **41**, 2837–2853 (2013).
Tokarska, K. B., Hegerl, G. C., Schurer, A. P., Ribes, A. & Fasullo, J. T. Quantifying human contributions to past and future ocean warming and thermosteric sea level rise. *Environ. Res. Lett.* **14**, 074020 (2019).

Input parameter	Mean value (GHG-only)	Mean value and [5-95%] range GHG-attributable (after adjusting by scaling factors)	Comments	Used in:
Radiative forcing for doubling of atmospheric CO_2 concentration $F_{2\times CO_2}$	3.7 ± 0.3 W/m²	3.7 ± 0.3 W/m²	The same for all cases, independent on time period	All cases
Greenhouse-gas only radiative forcing ΔF_{GHG}	2.33 [± 20%] W/m² 1.94 [± 20%] W/m²	2.33 [± 20%] W/m² 1.94 [± 20%] W/m²	Slope over the period multiplied by the time period length: 1862-2012 1955-2012	Case A1, A2 Case B1, B2,
Greenhouse-gas attributable surface warming ΔT_{GHG} (multi-model mean adjusted by β_{GHG})	1.47°C 1.33°C	1.14 [0.76, 1.53] °C † 1.03 [0.69, 1.38] °C †	Slope over the given period multiplied by the length of the time period: 1862-2012 1955-2012 †using β_{GHG} derived for 1862-2012	Case A1 Case B1
Greenhouse-gas attributable surface warming ΔT_{GHG} (multi-model mean adjusted by β_{GHG} with double variance)	1.47°C 1.33°C	1.14 [0.59, 1.70] °C † 1.03 [0.54, 1.54] °C †	Slope over the given period multiplied by the length of the time period: 1862-2012 1955-2012 †using β_{GHG} derived for 1862-2012	Case A2 Case B2
Greenhouse-gas attributable ocean heat content ΔN_{GHG} (multi-model mean adjusted by β_{GHG})	0.28 W/m² 0.60 W/m²	0.26 [0.17, 0.38] W/m² * 0.57 [0.36, 0.79] W/m² *	Slope over the period: 1862-2012* 1955-2012* *using β_{GHG} derived for 1955-2012 only	Case A Case B
Greenhouse-gas attributable ocean heat content ΔN_{GHG} (multi-model mean adjusted by β_{GHG} with double variance)	0.28 W/m² 0.60 W/m²	0.26 [0.13, 0.42] W/m² * 0.57 [0.27, 0.89] W/m² *	Slope over the period: 1862-2012* 1955-2012* *using β_{GHG} derived for 1955-2012	Case A2 Case B2

Supplementary Table S3. Values used in the input distributions to sample Eq. 3 and Eq.4 (Methods, Section 2.2; results in Section 3.3).

Radiative forcing data for ΔF_{GHG} was taken from historical scenario input for CMIP6.

1862-2012 period*		Resulting $S_{hist_{GHG}}$ [in K]			
Case name	Prior on $S_{hist_{GHG}}$	Most likely (at the maximum of pdf)	Median (50%)	17-83% range	5-95% range
A1 **Box model**	Implicit (unknown)	1.92	2.03	1.56 - 2.59	1.26 - 3.08
A1 **Forward model**	0 to 10 K	2.02	2.07	1.59 - 2.64	1.26 - 3.09
A2 **Box model** **(double noise)**	Implicit (unknown)	1.99	2.03	1.42 - 2.75	1.01 - 3.27
A2 **Forward model** **(double noise)**	0 to 10 K	1.98	2.09	1.45 - 2.82	1.00 - 3.40

*using β_{GHG} derived for 1862-2012 for ΔT_{GHG}, and β_{GHG} derived for 1955-2012 for ΔN_{GHG}
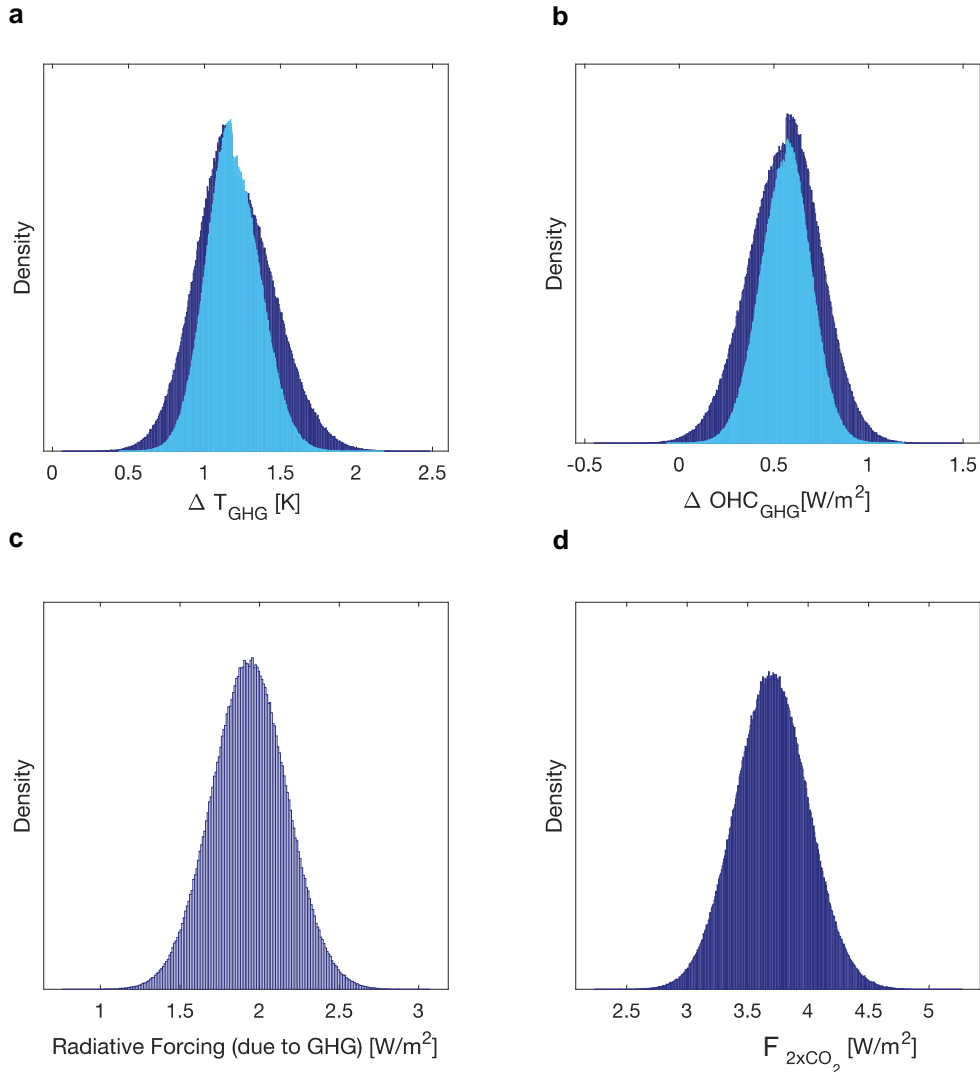
1955-2012 period*		Resulting $S_{hist_{GHG}}$ [in K]			
Case name	Prior on $S_{hist_{GHG}}$	Most likely (at the maximum of pdf)	Median (50%)	17-83% range	5-95% range
B1 **Box model**	Implicit (unknown)	2.61	2.77	2.08 - 3.69	1.66 - 4.58
B1 **Forward model**	0 to 10 K	2.65	2.87	2.13 - 3.82	1.67 - 4.68
B2 **Box model** **(double noise)**	Implicit (unknown)	2.53	2.77	1.88 - 3.93	1.34 - 5.10
B2 **Forward model** **(double noise)**	0 to 10 K	2.63	2.93	1.97 - 4.21	1.34 - 5.42

*using β_{GHG} derived for 1862-2012 for ΔT_{GHG}, and β_{GHG} derived for 1955-2012 for ΔN_{GHG}

Supplementary Table S4. Resulting values of the effective climate sensitivity ($S_{hist_{GHG}}$) for different cases and different choices of priors. (Please note that the numbers in the main text are reported with the first decimal place only, and rounded accordingly). For definition of each case see Supplementary Table S3 above.
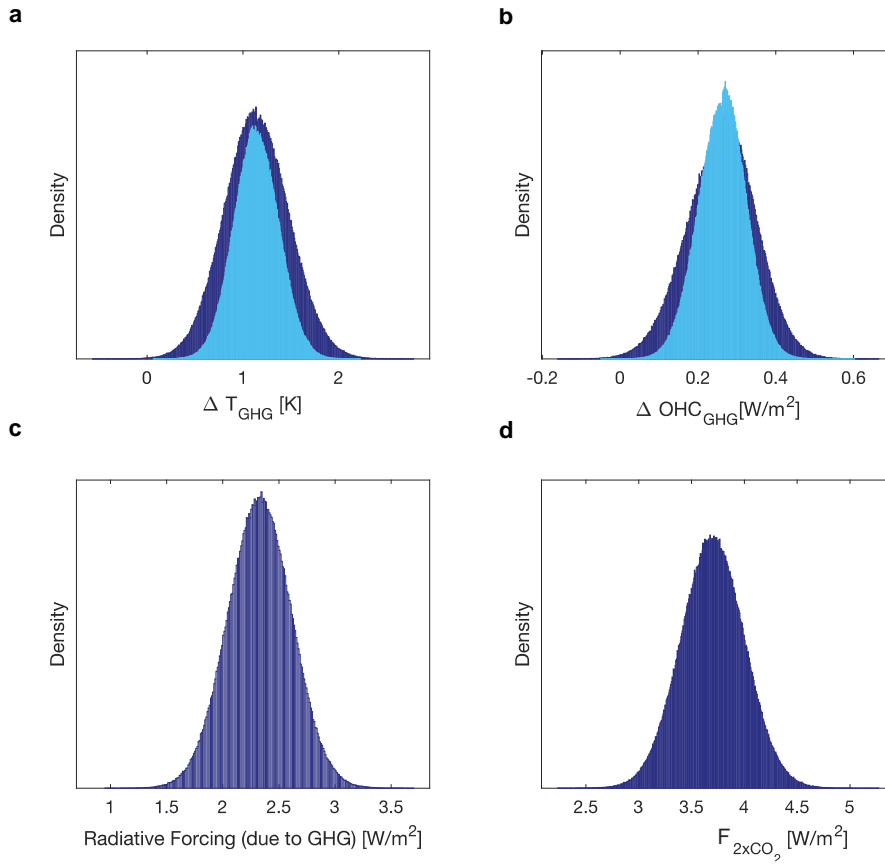
Supplementary Figure S1. Illustration of the input distributions to sample Eq. 3 and Eq.4, described in Supplementary Table S3, for the period 1862-2012. The distributions for ΔT_{GHG} and ΔN_{GHG} include a 'double-noise case' (panels a and b), indicated in dark blue, where the multi-model mean was adjusted by β_{GHG} with double variance (as in Supplementary table S3), and regular noise case (light blue). Panels (c) and (d) did not include the double noise option, thus, the same distributions were sampled from in all cases. (Distributions in panels (a) and (b) are a result from two Gaussians that were fitted individually (to the mean and 5th percentile, and mean and 95th percentile), after which they were joined, resulting in joint half-Gaussian distributions (flipped), as described below on p.8).

a

Density

$\Delta \, T_{GHG}$ [K]

b

Density

$\Delta \, OHC_{GHG}$ [W/m^2]

c

Density

Radiative Forcing (due to GHG) [W/m^2]

d

Density

F_{2xCO_2} [W/m^2]

Supplementary Figure S2. Illustration of the input distributions to sample Eq. 3 and Eq.4, described in Supplementary Table S3, for the period 1955-2012. The distributions for ΔT_{GHG} and ΔN_{GHG} include a 'double-noise case' (panels a and b), indicated in dark blue, where the multi-model mean was adjusted by β_{GHG} with double variance (as in Supplementary table S3), and regular noise case (light blue). Panels (c) and (d) did not include the double noise option, thus, the same distributions were sampled from in all cases. (Distributions in panels (a) and (b) are a result from two Gaussians that were fitted individually (to the mean and 5th percentile, and mean and 95th percentile), after which they were joined, resulting in joint half-Gaussian distributions (flipped), as described below on p.8).

The distributions were obtained by fitting a Gaussian distribution to the respective mean values and 5-95% ranges (Supplementary table S3). To obtain an estimate of the Gaussian distribution from a mean value (μ) and 5-95% range (i.e. the values of 5th percentile (val_5) and 95th percentile (val_95) are known, as in Supplementary Table S3). We make use of the critical value (z-score or z-value) for a 90% confidence interval (CI), which is equivalent to the 5-95% range (i.e. 90% of the population inside). Therefore, z= 1.644854 (often approximated to z=1.645 for 90% CI; that value can be obtained from a statistical table of z-values). If 95th percentile has value of val_95, then σ can be estimated as σ=(val_95 - μ)/Z, and a Gaussian distribution can be fitted using the mean (μ)and derived σ values. For a symmetric distribution, the 5th percentile and 95th percentile are the same, so the above procedure can be done once to obtain the input Gaussian distribution (Supplementary Figure S1; panels c,d). If the range was not symmetric, first, two Gaussians were fitted individually (to the mean and 5th percentile, and mean and 95th percentile), after which they were joined, resulting in joint half-Gaussian distributions (e.g. Supplementary Figure S1 panels a, b). Since the differences between the individual Gaussians are small, this asymmetry is barely visible, and such treatment does not make much difference to our final results.